Journal of Applied Physics ARTICLE scitation.org/journal/jap

A numerical modeling of the frequency dependence of the capacitance–voltage and conductance–voltage characteristics of GaN MIS structures

Cite as: J. Appl. Phys. **132**, 175302 (2022); doi: 10.1063/5.0112198
Submitted: 20 July 2022 · Accepted: 10 October 2022 ·
Published Online: 3 November 2022

K. Nishiguchi,[1,a)] K. Nakata,[1] and T. Hashizume[2]

AFFILIATIONS

[1]Transmission Devices Laboratory, Sumitomo Electric Industries, Ltd., Yokohama 244-8588, Japan
[2]Graduate School of Information and Science Technology and Research Center for Integrated Quantum Electronics (RCIQE), Hokkaido University, Sapporo 060-8628, Japan

[a)]**Author to whom correspondence should be addressed:** nishiguchi-kenya@sei.co.jp

ABSTRACT

The capacitance–voltage (C–V) and conductance–voltage (G–V) characteristics of GaN metal–insulator–semiconductor (MIS) structures have a frequency dependence due to the capture and emission of electrons by the high density of the interface states. However, the details of how an interface state affects C–V and G–V characteristics is still not well understood. In this paper, we report a numerical modeling method that can simulate the frequency dependent C–V and G–V characteristics of GaN MIS structures.

I. INTRODUCTION

A free-standing GaN substrate with a low dislocation density has become commercially available, due to the remarkable progress of crystal growth technology.[1] Progress on such homo-epitaxial growth technology has promoted the development of vertical-type GaN metal–insulator–semiconductor field-effect transistors (GaN MISFETs).[2–4] One of the most suitable insulating materials widely applied to GaN devices is Al_2O_3, which exhibits large band offset and high permittivity.[5–10]

Understanding and controlling the MIS interface is essential to improving the performance and stability of GaN MISFETs. GaN MIS structures generally have high density interface states, and many research groups have investigated and reported on their electrical properties.[11–13] The most common method to investigate interface states is the Terman method based on high frequency (>1 MHz) C–V characteristics, where there are no electron emissions from the interface states.[14] However, there are few detailed reports of the frequency dependence of the C–V and G–V characteristics. The reason for this is that there are few reports discussing frequency-dependent C–V and G–V characteristics simulation models.[15]

In this paper, we report the development of a numerical modeling method that can simulate the frequency dependency characteristics of the C–V and G–V of insulator/n-GaN structures with high accuracy. In addition, frequency dependent C–V and G–V characteristics are also calculated using TCAD and compared with our model. The interface state model is based on the disorder-induced gap state (DIGS) model proposed by Hasegawa and Ohno[16] and Hashizume and co-workers.[17] Using this method, we succeeded in reproducing the C–V and G–V characteristics of a Al_2O_3/n-GaN structure precisely. Finally, we used this method to predict the interface state density distribution at which the effect of electron capture and emission becomes almost negligible.

II. DEVICE STRUCTURE AND FABRICATION PROCESS

The Al_2O_3/n-GaN MIS structure is shown in Fig. 1. We used a 4 μm-thick homo-epitaxial Si-doped GaN layer grown on an n^+-GaN substrate with relatively low dislocation density ($< 3 \times 10^6\,cm^{-2}$). The donor density is $6.2 \times 10^{16}\,cm^{-3}$, which was determined by a C–V method using a Schottky diode. After the pre-treatment of the n-GaN surface in a 30%-HF solution for

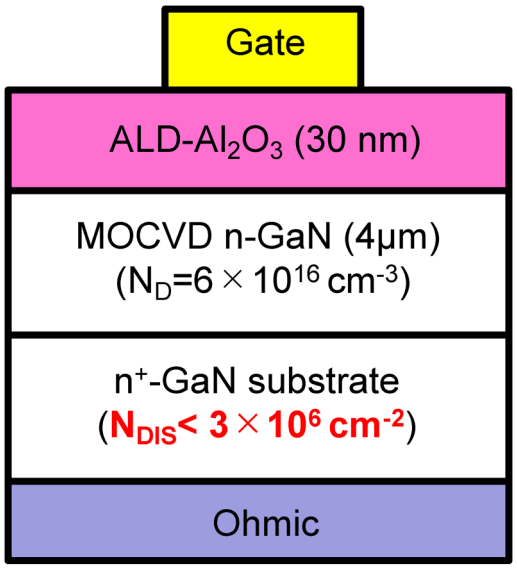

FIG. 1. Schematic illustration of a Al_2O_3/n-GaN MIS diode fabricated on a GaN substrate.

1min, a Al_2O_3 layer with a nominal thickness of 30 nm was deposited on the n-GaN surface using an ALD system (SUGA-SAL1500) at 300 °C. In the deposition process, water vapor and trimethylaluminum were introduced into a reactor in alternate pulse forms. Each precursor was injected into the reactor for 15 ms, and the purging time was set to 5 s. In this case, the deposition rate is 0.11 nm/cycle, indicating the formation of Al_2O_3 in a layer-by-layer fashion. A circular Ni/Au (=20/50 nm) with a diameter of 200 μm was deposited on the Al_2O_3 surface as a gate electrode.

The *C*–*V* and *G*–*V* characteristics of the Ni/Al_2O_3/n-GaN diode were measured at room-temperature (RT) as shown in Fig. 2(a). The frequency dependence of the *C*–*V* and *G*–*V* curves was caused by the capture and emission of electrons due to interface states. Figure 2(b) shows the interface state density distribution at the Al_2O_3/n-GaN interface determined by applying the Terman method to a 1 MHz *C*–*V* curve.[14] Note that the time constant of electron emission is extremely long at RT for interface states with deep energy levels relative to the conduction band edge. At RT, electron emission from E_C—0.8 eV takes 1000 s and from E_C—1.0 eV takes 1 year.[17] We thus plotted the evaluated data within the range of E_C—0.8 eV in Fig. 2(b). The sample exhibited relatively high state densities in the range of 10^{12} cm^{-2} eV^{-1}. In addition, a peak corresponding to a density of 2×10^{12} cm^{-2} eV^{-1} appeared at around E_C—0.6 eV, probably arising from a discrete trap related to nitrogen-vacancy defects.[6,18,19]

III. TCAD SIMULATION

We used small-signal analysis of SILVACO's ATLAS to simulate *C*–*V* and *G*–*V* characteristics.[20,21] We also used the intdefect function of ATLAS to set interface states.[22] The parameters are

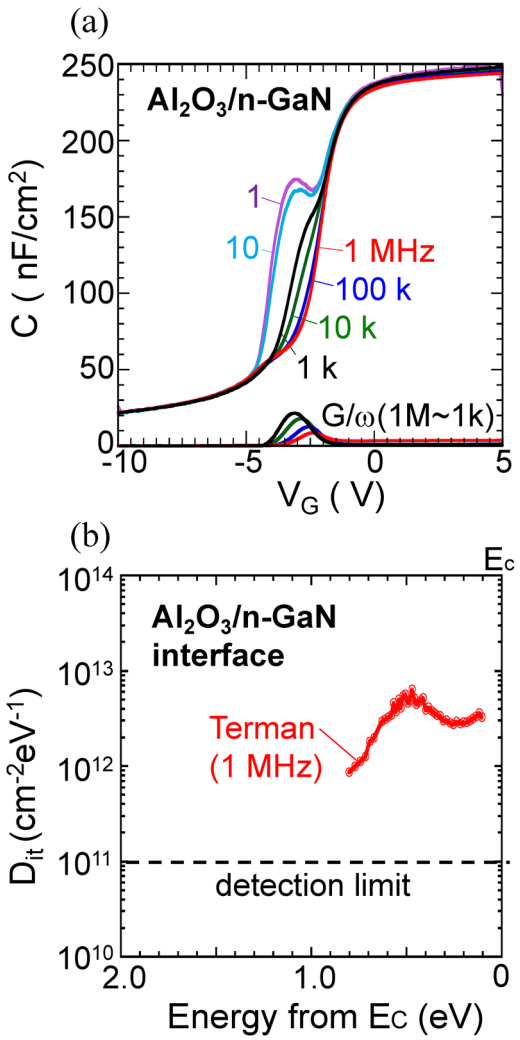

FIG. 2. (a) Room-temperature (RT) *C*–*V* and *G*–*V* characteristics of the MIS diode fabricated on the GaN substrate. (b) Interface state density (D_{it}) distribution determined by applying the Terman method to 1 MHz *C*–*V* measurement result.

described in Table I. The simulated *C*–*V* and *G*–*V* results are shown in Fig. 3(a). Figure 3(b) shows the interface state density distribution used in the TCAD simulation and agrees with the measured distribution [Fig. 2(b)]. The behavior of the frequency dispersion of the *C*–*V* and *G*–*V* simulation results is similar to the measurement results as shown in Fig. 2(a). Especially at the 1 and 10 Hz *C*–*V* curves, the behavior is very similar to the measurement data. However, bumps appear in the *C*–*V* curve at the 1 kHz–1 MHz which are not in the measurement results. In addition, *G*–*V* curves are twice larger the measurement values. These features indicate that small-signal analysis added an excess to the effects of the capture and emission of electrons to capacitance and conductance.

TABLE I. Parameters used in the TCAD simulation.

Parameter name	Symbol (unit)	Numerical value
Relative permittivity	$\varepsilon_{Al_2O_3}$	8.5[a]
Capture cross section of interface states intdefect parameters	σ (cm^2)	1×10^{-16}[b]
	nta (cm^{-2})	6.5×10^{12}
	wta	0.22
	ngd (cm^{-2})	5.1×10^{12}
	egd (eV)	2.9
	wgd	0.2
Temperature	*T* (K)	300

[a]Reference 23.
[b]At Al_2O_3/GaN interface.[24]

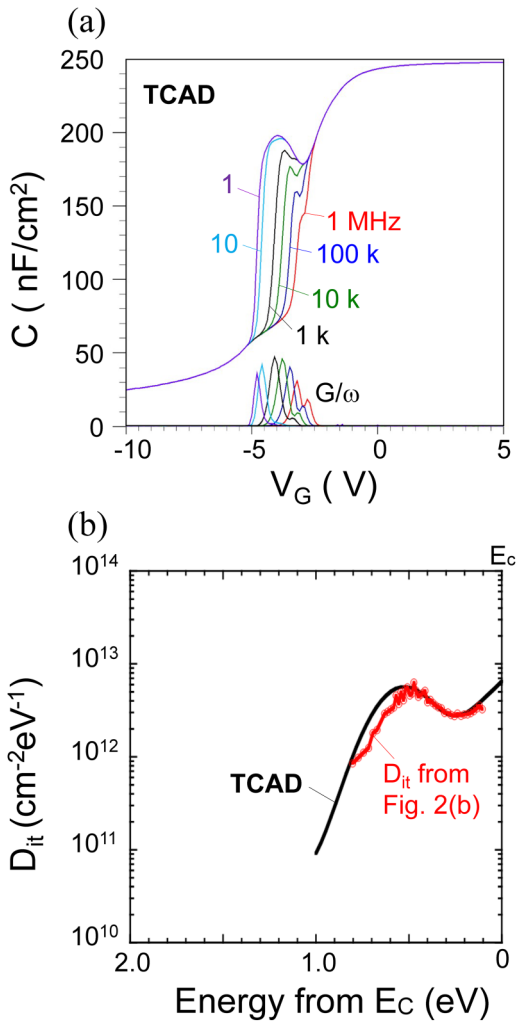

FIG. 3. (a) *C–V* and *G–V* characteristics of TCAD simulation. (b) Interface state density (D_{it}) distribution used in the simulation.

IV. NUMERICAL MODELING METHOD

We developed a modeling method that combines potential simulation and equivalent circuit calculation to calculate *C–V* and *G–V* characteristics. The potential distribution and equivalent circuit of the Al_2O_3/n-GaN structure with interface states is shown in Fig. 4. $C_{Al_2O_3}$ is the capacitance of the Al_2O_3, and C_{GaN} is the capacitance of the n-GaN. Charging and discharging of electrons due to interface states are represented by C_{it} and G_{it} connected in parallel to C_{GaN}.[25] C_{it} and G_{it}, which cannot follow the AC signal, and are almost zero and are ignored.[26] The total capacitance *C* and total conductance *G* of the circuit are calculated as follows:

$$G_{Ptot} = \int_{E_V}^{E_C} \frac{\omega^2 C_{it}(E)\tau_{it}(E)}{1+\omega^2\tau_{it}(E)^2}\, dE, \tag{1}$$

$$C = C_{Al_2O_3}\frac{\left(\frac{G_{Ptot}}{\omega}\right)^2 + (C_{GaN}+\alpha)\beta}{\left(\frac{G_{Ptot}}{\omega}\right)^2 + \beta^2}, \tag{2}$$

$$\begin{aligned} G &= G_{Ptot}\frac{C_{Al_2O_3}^2}{\left(\frac{G_{Ptot}}{\omega}\right)^2+\beta^2}, \\ \alpha &= \int_{E_V}^{E_C}\frac{C_{it}(E)}{1+\omega^2\tau_{it}(E)^2}\, dE, \\ \beta &= C_{Al_2O_3} + C_{GaN} + \alpha, \end{aligned} \tag{3}$$

where ω is the angular frequency and $\tau_{it}(E)$ is the time constant of the electron emission from the energy calculated by the SRH model.[27] $C_{Al_2O_3}$, ω, and $\tau_{it}(E)$ are expressed as follows:

$$C_{Al_2O_3} = \frac{\varepsilon_{Al_2O_3}}{d_{Al_2O_3}}, \tag{4}$$

$$\omega = 2\pi \cdot freq, \tag{5}$$

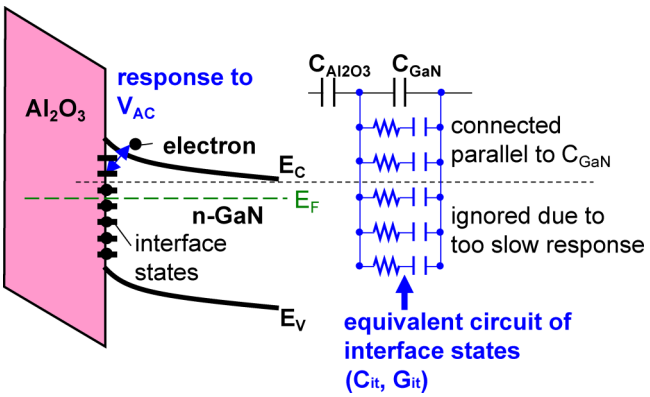

FIG. 4. Schematic illustration of the potential distribution and the equivalent circuit of the Al_2O_3/n-GaN structure with interface states.

$$\tau_{it}(E) = \frac{1}{N_C \nu \sigma} \exp\left(\frac{E_C - E}{kT}\right), \tag{6}$$

where $\varepsilon_{Al_2O_3}$ and $d_{Al_2O_3}$ are the permittivity and thickness of the Al_2O_3 layer, *freq* is the measurement frequency, N_C is the effective density of states in the conduction band of n-GaN, ν is the thermal velocity of electrons, σ is the capture cross section of the interface states, $E_C - E$ is the energy depth from the conduction band edge, and k and T are the Boltzmann constant and temperature, respectively.

C_{GaN} and $C_{it}(E)$ are obtained by solving potential calculations using the Poisson equation. Figure 5 shows the flow of the potential simulation using the Poisson equation with an elaborate computer program. V_G is the DC voltage and ΔV_{AC} is the voltage of the AC signal of the C–V measurement. In this paper, ΔV_{AC} is 20 mV. The n-GaN accumulates electrons and the interface states capture electrons at (a) in Fig. 5. The n-GaN releases electrons at (b) in Fig. 5. C_{GaN} is calculated using the difference of the total carrier density of the n-GaN (ΔQ_{GaN}) between (a) and (b) as follows:

$$C_{GaN} = \frac{\Delta Q_{GaN}}{2\Delta V_{AC}}. \tag{7}$$

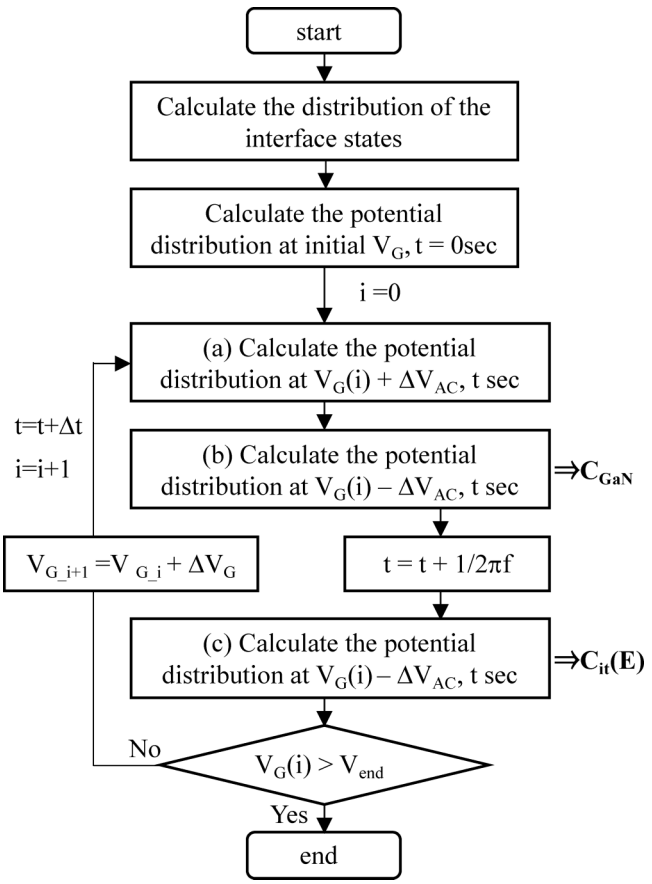

FIG. 5. Simulation flow.

Q_{GaN} is calculated as follows:

$$Q_{GaN} = q n_{tot}, \tag{8}$$

where n_{tot} is the total electron density n of the n-GaN layer. Since there is no time lapse from (a) to (b) in Fig. 5, there is no electron emission from the interface states. On the other hand at (c) in Fig. 5, $\Delta Q_{it}(E)$ is the calculated electron emission from the interface states. $C_{it}(E)$ is calculated as follows:

$$C_{it}(E) = \frac{\Delta Q_{it}(E)}{2\Delta V_{AC}}. \tag{9}$$

We assume that in the n-GaN layer, Poisson's equation takes the form

$$\frac{d^2\psi}{dx^2} = -\frac{q}{\varepsilon_0 \varepsilon_{GaN}}(N_D - n), \tag{10}$$

where ψ, ε, ε_{GaN}, and N_D are the electric potential, the vacuum permittivity, the relative permittivity of GaN, and N_D is the concentration of fully ionized donor dopants. Furthermore, we assumed that in the insulator layer this equation becomes Laplace's equation,

$$\frac{d^2\psi}{dx^2} = 0. \tag{11}$$

Equations (10) and (11) were solved self-consistently using the finite element Successive Over-Relaxation method with the following boundary conditions:[28]

- Dirichlet type boundary conditions at the contacts.
- Neumann type boundary conditions at the Al_2O_3/n-GaN interface determined by the density of the interface charge. In particular, the boundary conditions at the Al_2O_3/n-GaN interface are expressed as[24]

$$\varepsilon_0 \varepsilon_s \left.\frac{d\psi}{dx}\right|_s - \varepsilon_0 \varepsilon_I \left.\frac{d\psi}{dx}\right|_I = Q_{fix} + \int_{E_V}^{E_C} Q_{it}(E)\, dE, \tag{12}$$

where ε_I is the insulator dielectric constant and Q_{fix} is the interface fixed charge and $Q_{it}(E)$ is expressed as follows:

$$\begin{aligned} Q_{it}(E) = q\big(&D_{it}^{D}(E)(1 - f_0(E)(1 - \eta_e(E,t)) - \eta_e(E,t) f(E)) \\ &- D_{it}^{A}(E)(f_0(E)(1 - \eta_e(E,t)) + \eta_e(E,t) f(E))\big), \end{aligned} \tag{13}$$

where E_C is the conduction band minimum, E_V is the valence band maximum, D_{it}^{D} and D_{it}^{A} are the density of donor-like and acceptor-like states, $f(E)$ and $f_0(E)$ are the Fermi–Dirac function at the current state and the previous state. $\eta_e(E, t)$ describes the probability of electron emission from the trap at energy E and can be calculated as follows:[27]

$$\eta_e(E, t) = 1 - \exp\left(\frac{-t}{\tau_{it}(E)}\right). \tag{14}$$

In the calculations, we assumed two types of energetic distribution of electronic state density at the insulator/semiconductor

interface. One type of $D_{it}(E)$ is a U-shaped distribution in accordance with a disorder-induced gap state model with donor-like states below the charge neutrality level E_{CNL} and acceptor-like states above it.[16,17,29] The density of the states reaches the minimum, denoted as D_{it0}, at E_{CNL}, and the full formula for $D_{it}(E)$ is

$$D_{it}^{A,D}(E) = D_{it0}\exp\left[\left(\frac{|E - E_{CNL}|}{E_{0A,0D}}\right)^{n_{A,D}}\right], \quad (15)$$

where E_{0A}, n_A, E_{0D}, and n_D describe the curvature of the acceptor-like branch ($E_{CNL} < E < E_C$) and the donor-like one ($E_V < E < E_{CNL}$), respectively.[17,24] The other kind of $D_{it}(E)$ is a narrow Gaussian curve describing defect discrete states,

$$D_{it\_Discrete}^{A,D}(E) = D_{it\_max}\exp\left[-4\log 2\left(\frac{E - E_{A,D}}{\mathrm{FWHM}}\right)^2\right] \quad (16)$$

where D_{it_max} is the maximum density, $E_{A,D}$ is the energetic location of the level, and FWHM is the full width at half maximum of the Gaussian curve.[24] The potential distributions were calculated by solving Eqs. (10)–(16).

TABLE II. Parameters used in the numerical modeling simulation.

Parameter name	Symbol (unit)	Numerical value
The effective density of states	N_C (cm^{-3})	2.24×10^{18}
The thermal velocity of electrons	v (cm/sec)	2.6×10^{7}
Relative permittivity	ε_{GaN}	9.5
	$\varepsilon_{Al_2O_3}$	8.5[a]
Band offset	ΔE_C (eV)	2.4[b]
Donor concentration	N_D (cm^{-3})	5×10^{16}
Surface barrier height	ϕ_s (eV)	3.4[c]
Charge neutrality level	E_{CNL}	$E_C - 1.3$ eV[d]
Capture cross section of interface states	σ (cm^2)	1×10^{-16}[e]
The interface fixed charge	Q_{fix} (cm^{-2})	7.1×10^{12}
DIGS model parameters	D_{it0} (cm^{-2})	1.5×10^{12}
	$E_{0A,0D}$ (eV)	4.26
	n_A	6
	n_D	3
	D_{it_max} (cm^{-2})	4.0×10^{12}
	E_A (eV)	0.49
	FWHM (eV)	0.28
Total time	t (s)	100
Temperature	T (K)	300

[a]Reference 23.
[b]At Al_2O_3/GaN interface.[11]
[c]At Ni/Al_2O_3 interface.[30]
[d]At Al_2O_3/GaN interface.[29]
[e]At Al_2O_3/GaN interface.[24]

V. SIMULATION RESULTS

The simulated C–V and G–V curves made by using the proposed numerical method and the parameters described in Table II are shown in Fig. 6(a). Q_{fix} is a positive value because there is a possibility that defect levels produce excess positive charges in the Al_2O_3 layer.[31,32] The interface state density distribution used in this calculation is shown in Fig. 6(b) and agrees with the measured distribution [Fig. 2(b)].

The simulated C–V and G–V curves are very similar to the measured curves as shown in Fig. 2(a). Frequency response of the energy depth calculated by using Eq. (14) is shown in Fig. 6(b). No electron is emitted from the discrete level at 1 MHz, but electrons fully responded at 1 Hz. Thus, at low frequencies, C is increased with the addition of parallel C_{it}, as shown in Fig. 4. And at high frequencies, no bumps appear in the C–V curve at 1 kHz–1 MHz unlike TCAD simulation result [Fig. 3(a)]. This is because $(1+\omega^2\tau_{it}(E)^2)$ becomes larger at high frequencies in α in Eqs. (1)–(3), which reduces the effect of $C_{it}(E)$. Therefore, the numerical

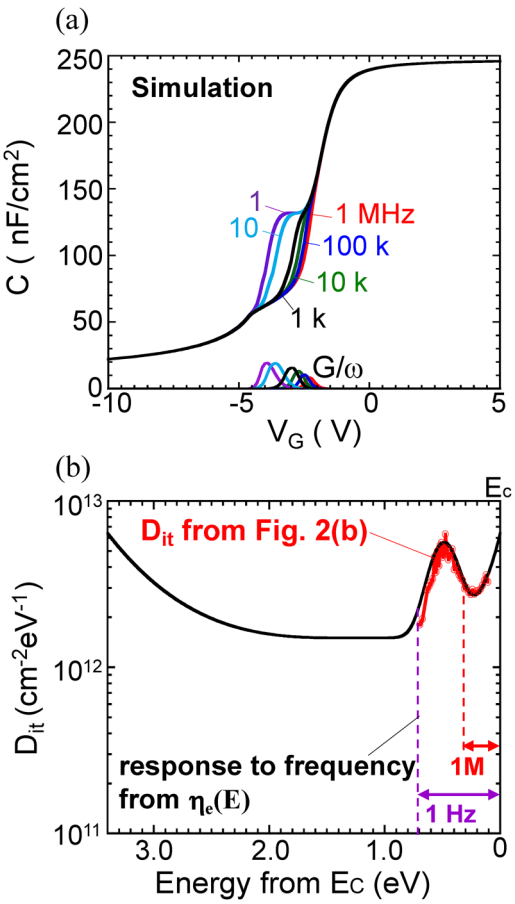

FIG. 6. (a) C–V and G–V simulations of the MIS diode. (b) D_{it} distribution used for the simulations.

modeling method can prevent excessive addition of the effect of capture and emission electron due to interface states.

In addition, the peak values of each G/ω shift toward a positive gate bias at higher frequencies in simulation results [shown in Fig. 6(a)], and the behavior is very similar to the measured data [shown in Fig. 2(a)]. We analyzed this phenomenon mathematically. $G_P(E)/\omega$ is expressed by Eq. (1) as follows:

$$\frac{G_{Ptot}}{\omega} = \int_{E_V}^{E_C} C_{it}(E)\frac{G_P(E)}{\omega}\,dE, \tag{17}$$

$$\frac{G_P(E)}{\omega} = \frac{\omega\tau_{it}(E)}{1+\omega^2\tau_{it}(E)^2}. \tag{18}$$

As the frequency increases, the peaks of each $G_P(E)/\omega$ approach E_C as shown in Fig. 7(a). As the gate bias increases, the energy of the interface states responding to V_{AC} approaches E_C as shown in Fig. 4, so the shift of G/ω peaks is attributed to that of $G_P(E)/\omega$. These results proved that the numerical modeling method can simulate C–V and G–V characteristics of GaN MIS structures with high accuracy and give a detailed analysis.

On the other hand, frequency dispersion of the simulated C–V curves are compact and the simulated G–V curves are sharp

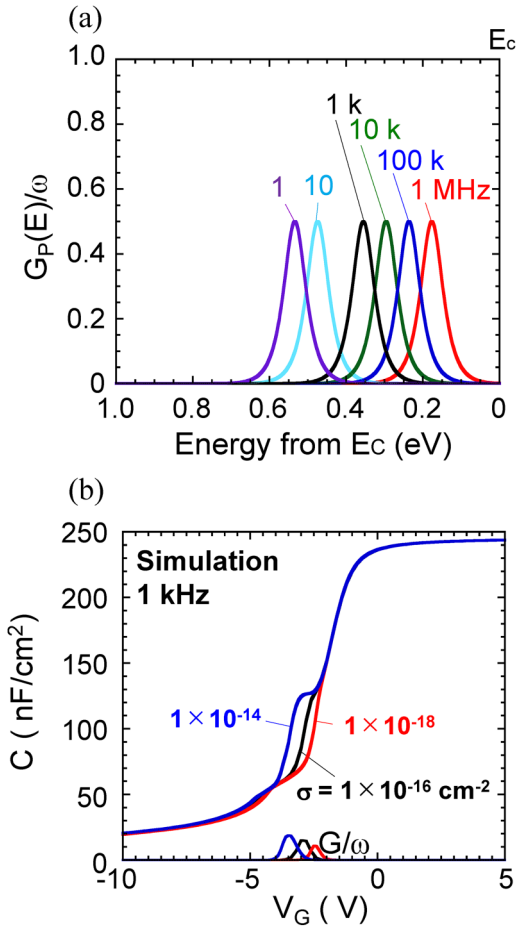

FIG. 7. (a) Frequency dependence of the $G_P(E)/\omega$. (b) Correlation between capture cross section and C–V and G–V characteristics.

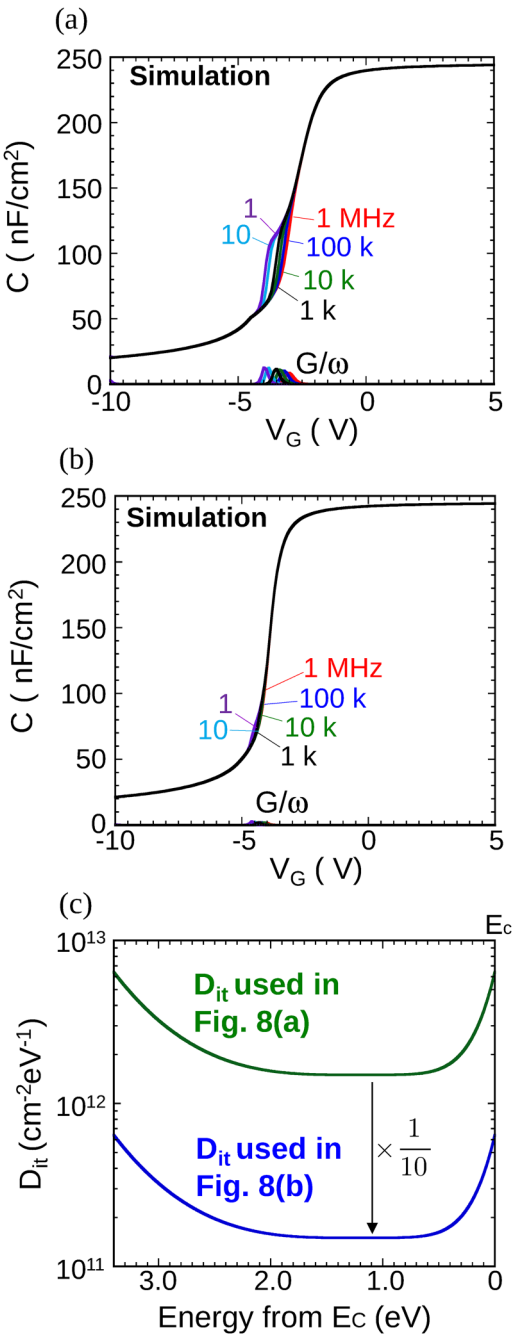

FIG. 8. (a) C–V and G–V simulation without nitrogen-vacancy. (b) C–V and G–V simulation with low D_{it}. (c) D_{it} distribution used for the simulations.

compared to the measurement values. To analyze this phenomenon, we investigated the correlation between the capture cross section and C–V and G–V characteristics [Fig. 7(b)]. The G–V curve shifts to a negative V_G and the capacitance is increased due to the interface states as the capture cross section is increased. Conversely, the G–V curve shifts to a positive V_G and the capacitance is decreased due to the interface states as the capture cross section is decreased. Therefore, if the capture cross section has some variation, the C–V and G–V curves are expected to be broad toward both negative and positive V_G and would be closer to the measurement results.

Finally, we calculated the C–V and G–V characteristics using this numerical model with low density of interface states. Figure 8(a) shows the C–V and G–V curves with D_{it} shown in Fig. 8(c). D_{it} is equal to the one shown in Fig. 6(b) without the discrete level. The frequency dependence of the C–V and G–V curves in Fig. 8(a) is greatly suppressed. This result indicates that the frequency dependence of the C–V and G–V characteristics can be greatly reduced by eliminating nitrogen-vacancy. Figure 8(b) shows almost no frequency dispersion in the C–V and G–V curves. These results indicate that when the interface states density is less than $10^{12}\ \mathrm{cm}^{-2}\ \mathrm{eV}^{-1}$, the interface states have little effect on the C–V and G–V characteristics.

VI. CONCLUSION

We developed a numerical modeling method, which can simulate the frequency dependent C–V and G–V characteristics of GaN MIS structures. Frequency dependent C–V and G–V characteristics of the Al_2O_3/n-GaN MIS diode were simulated by using our model. The simulated C–V and G–V curves reproduced the experimental data better than the TCAD simulation results. Finally, we showed the relationships of C–V and G–V characteristics with low density of the interface states. To suppress the frequency dispersion of the C–V and G–V characteristics, the interface state density must be less than $10^{12}\ \mathrm{cm}^{-2}\ \mathrm{eV}^{-1}$.

AUTHOR DECLARATIONS

Conflict of Interest

The authors have no conflicts to disclose.

Author Contributions

K. Nishiguchi: Conceptualization (lead); Data curation (lead); Formal analysis (lead); Investigation (lead); Methodology (lead); Project administration (lead); Resources (lead); Software (lead); Validation (lead); Visualization (lead); Writing – original draft (lead); Writing – review & editing (lead). **K. Nakata:** Funding acquisition (equal); Supervision (equal). **T. Hashizume:** Formal analysis (lead); Investigation (supporting); Project administration (supporting); Resources (equal); Validation (supporting); Visualization (lead).

DATA AVAILABILITY

The data that support the findings of this study are available from the corresponding author upon reasonable request.

REFERENCES

[1]H. Fujikura, T. Konno, T. Kimura, Y. Narita, and F. Horikiri, Appl. Phys. Lett. **117**, 012103 (2020).
[2]M. Kodama, M. Sugimoto, E. Hayashi, N. Soejima, O. Ishiguro, M. Kanechika, K. Itoh, H. Ueda, T. Uesugi, and T. Kachi, Appl. Phys. Express **1**, 021104 (2008).
[3]T. Kachi, Jpn. J. Appl. Phys. **53**, 100210 (2014).
[4]T. Oka, Jpn. J. Appl. Phys. **58**, SB0805 (2019).
[5]C. Mizue, Y. Hori, M. Miczek, and T. Hashizume, Jpn. J. Appl. Phys. **50**, 021001 (2011).
[6]Y. Hori, C. Mizue, and T. Hashizume, Jpn. J. Appl. Phys. **49**, 080201 (2010).
[7]Z. Yatabe, Y. Hori, W.-C. Ma, J. T. Asubar, M. Akazawa, T. Sato, and T. Hashizume, Jpn. J. Appl. Phys. **53**, 100213 (2014).
[8]S. Kaneki, J. Ohira, S. Toiya, Z. Yatabe, J. T. Asubar, and T. Hazhizume, Appl. Phys. Lett. **109**, 162104 (2016).
[9]S. Ozaki, K. Makiyama, T. Ohki, N. Okamoto, S. Kaneki, K. Nishiguchi, N. Hara, and T. Hashizume, Appl. Phys. Express **10**, 061001 (2017).
[10]K. Nishiguchi, S. Kaneki, S. Ozaki, and T. Hashizume, Jpn. J. Appl. Phys. **56**, 101001 (2017).
[11]T. Hashizume, S. Ootomo, T. Inagaki, and H. Hasegawa, J. Vac. Sci. Technol. B **21**, 1828 (2003).
[12]T. Hashizume, S. Ootomo, and H. Hasegawa, Appl. Phys. Lett. **83**, 2952 (2003).
[13]Y. Hori, Z. Yatabe, and T. Hashizume, J. Appl. Phys. **114**, 244503 (2013).
[14]L. M. Terman, Solid-State Electron. **5**, 285 (1962).
[15]K. Fukuda, H. Asai, J. Hattori, M. Shimizu, and T. Hashizume, Jpn. J. Appl. Phys. **57**, 04FG04 (2018).
[16]H. Hasegawa and H. Ohno, J. Vac. Sci. Technol. B **4**, 1130 (1986).
[17]J. T. Asubar, Z. Yatabe, D. Gregusova, and T. Hashizume, J. Appl. Phys. **129**, 121102 (2021).
[18]T. Hashizume and R. Nakasaki, Appl. Phys. Lett. **80**, 4564 (2002).
[19]T. Hashizume and H. Hasegawa, Appl. Surf. Sci. **234**, 387 (2004).
[20]S. E. Laux, IEEE Trans. Electron. Devices **32**, 2028 (1985).
[21]L. Maresca, I. Matacena, M. Riccio, A. Irace, G. Breglio, and S. Daliento, IEEE J. Emerg. Sel. Top. Power Electron. **9**, 2171 (2021).
[22]Software D S 2016 ATLAS User's Manual, pp. 1060–1066.
[23]T. Hashizume, S. Kaneki, T. Oyobiki, Y. Ando, S. Sasaki, and K. Nishiguchi, Appl. Phys. Express **11**, 124102 (2018).
[24]M. Miczek, C. Mizue, T. Hashizume, and B. Adamowicz, J. Appl. Phys. **103**, 104510 (2008).
[25]E. H. Nicollian and J. R. Brews, *MOS (Metal Oxide Semiconductor) Physics and Technology* (Wiley, New York, 2003), p. 183.
[26]Y. Hori, Z. Yatabe, and T. Hashizume, J. Appl. Phys. **114**, 244503 (2013).
[27]W. Shockley and W. T. Read, Phys. Rev. **87**, 835 (1952) [R. N. Hall, *ibid* **87**, 387 (1952)].
[28]S. Yang and M. K. Gobbert, Appl. Math. Lett. **22**, 325 (2009).
[29]W. Mönch, J. Appl. Phys. **109**, 113724 (2011).
[30]E. Bersch, S. Rangan, and R. A. Bartynski, Phys. Rev. B **78**, 085114 (2008).
[31]P. Jonnard, C. Bonnelle, G. Blaise, G. Rémond, and C. Roques-Carmes, J. Appl. Phys. **88**, 6413 (2000).
[32]M. Choi, J. L. Lyons, A. Janotti, and C. G. Van de Walle, Phys. Status Solidi B **250**, 787 (2013).